Converging Cooperative Functions into the Nanospace of Covalent Organic Frameworks for Efficient Uranium Extraction from Seawater

Mengjie Hao[1], Zhongshan Chen[1], Xiaolu Liu[1], Xianhai Liu[1], Juyao Zhang[1], Hui Yang[1]*, Geoffrey I. N. Waterhouse[2], Xiangke Wang[1]* & Shengqian Ma[3]*

[1]College of Environmental Science and Engineering, North China Electric Power University, Beijing 102206, [2]MacDiarmid Institute for Advanced Materials and Nanotechnology, School of Chemical Sciences, The University of Auckland, Auckland 1142, [3]Department of Chemistry, University of North Texas, Denton, TX 76201

*Corresponding authors: h.yang@ncepu.edu.cn; xkwang@ncepu.edu.cn; shengqian.ma@unt.edu

The extraction of uranium from seawater is challenging though it offers tremendous potential for the sustainable production of nuclear fuel for the energy sector. Herein, we report a new strategy for efficient extraction of uranium from seawater via converging the cooperative functions of adsorption–photocatalysis into the nanospace of covalent organic frameworks (COFs). Functionalization of the organic linkers in the multicomponent COFs allowed exploration of the relationship between material composition and adsorption–photocatalytic activity for uranium extraction. The presence of amidoxime groups in the COFs offered selective binding sites for uranyl, whilst triazine units and bipyridine-Pd groups acted cooperatively to photocatalytically reduce adsorbed U(VI) to a U(IV) solid product (UO_2) for facile collection. One of our developed COFs, 4-Pd-AO, displayed exceptional performance in sequestering and reducing uranyl from natural seawater, with a high extraction capacity of 4.62 mg U/g per day (average data) under visible light irradiation. Mechanistic studies revealed that 4-Pd-AO not only reduced adsorbed uranyl(VI) to $U(IV)O_2$, but also generated $^1O_2$ and superoxide radicals under visible light excitation, thus affording excellent antibacterial and antialgal activities (i.e.,

antibiofouling properties) for sustained efficient uranium extraction performance. This proof-of-concept study establishes multicomponent COFs as promising candidates for efficient uranium extraction from seawater.
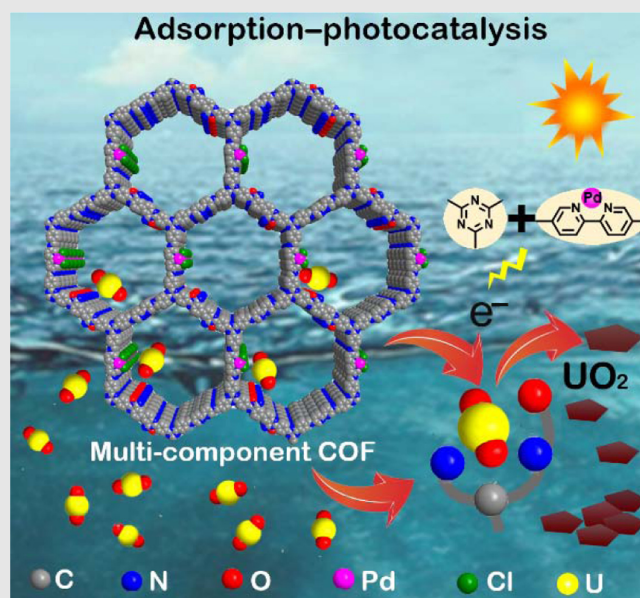
Keywords: covalent organic frameworks, seawater, uranium extraction, adsorption–photocatalysis, cooperativity

Introduction

Nuclear energy is expected to play an important role in the future decarbonization of the energy sector.[1,2] Enriched uranium is the fuel used in most fission-based nuclear reactors. The scarcity of uranium ore reserves on land (~4.5 million tons) is an obstacle to the long-term future of nuclear energy in beyond-fossil-fuel energy infrastructures.[3] However, uranium reserves in seawater are abundant, ~1000 times those on land.[4,5] Accordingly, the discovery of efficient technologies for the extraction of uranium from seawater is seen as a promising pathway for the sustained production of nuclear fuel.

To address this need, much effort has been focused on developing sorbents for uranium extraction, with essential requirements of such sorbents being high uranyl adsorption selectivity, rapid adsorption kinetics, large adsorption capacity, and reusability.[6] Traditional porous sorbents such as porous carbons,[7–12] mesoporous silica,[13] and layered inorganic materials[14] are limited in their usefulness because of the low density of functional groups that selectively bind U(VI) ions, generally leading to slow adsorption kinetics and poor adsorption capacities. Amorphous porous organic polymers (POPs) are possible candidates, but their performance is hampered by their disordered structures, which block the uranyl chelating sites.[15–24] As porous crystalline materials, metal–organic frameworks (MOFs) have been pursued for uranium extraction, stimulated by their high surface areas and well-defined/varied pore environments.[25–29] However, the modest stabilities of most MOFs in water limit their practical utility. Compared with traditional porous materials such as POPs, and MOFs, covalent organic frameworks (COFs) show particular promise as uranium adsorbents from seawater due to their uniform porosity, tunable chemical characteristics and functional groups, high surface area, physiochemical stability, and acid–base stability.[30–34] A number of works have shown that the introduction of amidoxime chelating groups into COF structures results in enhanced uranium extraction from seawater.[19,23,31,32,34–38] However, competitive metal ion adsorption can block some uranyl binding sites, resulting in blockage of the channels of the COFs and a reduction in the uranium adsorption capacity and hindering uranium recovery and adsorbent reuse. Furthermore, biofouling by marine bacteria and algae can also passivate sorbents in seawater, thus lowering the uranyl uptake capacity rapidly and in extreme cases completely suppressing adsorption.[39–41] To overcome these issues, the development of materials with fast kinetics, large capacities, high adsorption selectivities, and antibiofouling properties are crucial if COFs are to be of practical use for uranium extraction from seawater.

Recently, increasing interest has focused on the synthesis of COFs with photosensitive functional groups that can effectively promote photocatalytic reduction reactions.[42–46] This inspired us to develop an adsorption–photocatalytic strategy for uranium extraction from natural seawater. Our targeted strategy involved the synthesis of COFs with a high density of chelating moieties and abundant photoactive sites, thereby achieving effective uranyl binding kinetics, highly selective uranyl adsorption, a high adsorption capacity, uranyl reduction to a solid U(IV) product under visible light, and reactive oxygen species-mediated antibiofouling activity. COFs with such characteristics would solve the critical challenges of extracting uranium from natural seawater. Engineering the chemical microenvironment in multicomponent COF frameworks is critical to realize such broad-spectrum performance.

To implement this strategy, we engineered the pore structure of a multicomponent COF to contain amidoxime groups, triazine groups, and bipyridine-metal groups (Figure 1). This functionality was realized by incorporating the relevant functional moieties on the framework linkers. Through detailed experimental studies, the resultant COF (denoted herein as COF 4-Pd-AO) demonstrated excellent uranium extraction performance in spiked-seawater and natural seawater under visible light irradiation. The amidoxime groups imparted hydrophilicity and a high binding affinity for uranyl. The triazine groups and bipyridine-Pd(II) components served as duel photocatalytic active sites, which reduced U(VI) of uranyl to U(IV) in the form of solid
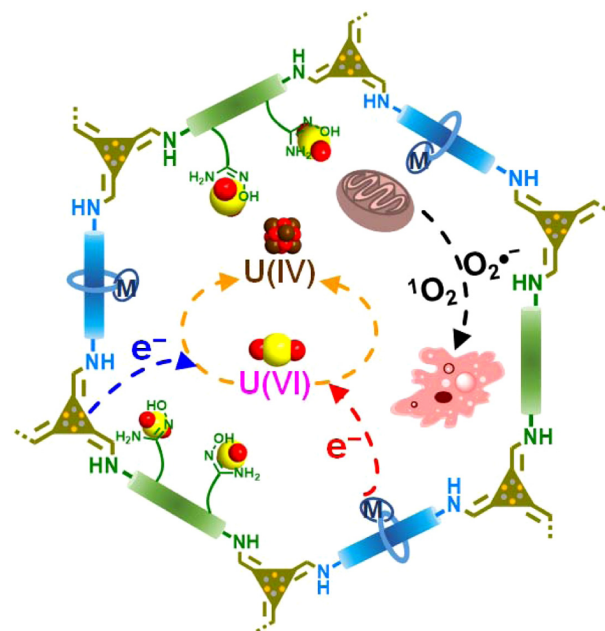

Figure 1 | *Adsorption–photocatalytic strategy for uranium extraction. Schematic of a multicomponent COF with chelating amidoxime moieties and photocatalytic active sites and antibiofouling ability as an adsorption–photocatalyst for uranium extraction from seawater.*

UO$_2$ for easy collection. Mechanistic studies revealed that O$_2$•$^-$ and ^{1}O$_2$ free radicals generated by the COF under light irradiation could damage the structure of marine bacteria and inhibit colonization by algae, imparting the multicomponent COF with excellent antibiofouling activity. Because of these features, COF 4-Pd-AO delivered a uranium uptake capacity of 4.62 mg/g per day (average data) in natural seawater using the adsorption–photocatalytic process. Our COF-based adsorption–photocatalytic strategy thus offers a promising new approach for uranium extraction from seawater.

Experimental Methods

Synthesis of COF 1

In a 5 mL glass tube, *p*-phenylenediamine (Pa, 8.6 mg), 2,2′-bipyridine-5,5′-diamine (Bpy, 7.5 mg), and 2,4,6-tri-formylphloroglucinol (Tp, 16.8 mg) were dissolved in 1.1 mL of a mixed solvent solution containing *o*-dichlorobenzene (*o*-DCB)/*n*-butyl alcohol (*n*-BuOH)/acetic acid (AcOH, 6 M) in a volume ratio of 5/5/1. The mixture was then frozen in a liquid nitrogen bath and sealed with a gas torch. The tube was then heated at 120 °C for 3 days, after which the product was washed several times with tetrahydrofuran (THF) and acetone, collected by vacuum filtration, and dried under vacuum at 40 °C overnight.

Synthesis of COF 2

In a 5 mL glass tube, 2,5-diaminobenzonitrile (Db, 10.6 mg), Bpy (7.5 mg), and Tp (16.8 mg) were dissolved in 1.1 mL of a mixed solvent solution of *o*-DCB/*n*-BuOH/AcOH (6 M) in a volume ratio of 5/5/1. The mixture was then frozen in a liquid nitrogen bath and sealed with a gas torch. The tube was then heated at 120 °C for 3 days, after which the product was washed several times with THF and acetone, collected by vacuum filtration, and dried under vacuum at 40 °C overnight.

Synthesis of COF 3

In a 5 mL glass tube, [1,1′-biphenyl]-3,3′-dicarboni-trile,4,4′-diamino- (Bpdba, 9.4 mg), Bpy (14.9 mg), and Tp (16.8 mg) were dissolved in 1.1 mL of a mixed solvent solution of *o*-DCB/*n*-BuOH/AcOH (6 M) in a volume ratio of 5/5/1. The mixture was then frozen in a liquid nitrogen bath and sealed with a gas torch. The tube was then heated at 120 °C for 3 days, after which the product was washed several times with THF and acetone, collected by vacuum filtration, and dried under vacuum at 40 °C overnight.

Synthesis of COF 4

In a 5 mL glass tube, 4,4′,4″-(1,3,5-triazine-2,4,6-triyl) tribenzaldehyde (TATTA, 31.5 mg), Bpy (14.9 mg) and

Bpdba (9.4 mg) were dissolved in 1.1 mL of a mixed solvent solution of *o*-DCB/dimethylacetamide/AcOH (6 M) in a volume ratio of 9/1/1. The mixture was then frozen in a liquid nitrogen bath and sealed with a gas torch. After being heated at 120 °C for 3 days, the product was washed several times with THF and acetone, collected by filtration, and dried under vacuum overnight.

Synthesis of COFs 2-AO, 3-AO, and 4-AO

For the synthesis of COF 2-AO (AO, amidoxime groups), 0.2 g of COF 2 was dispersed in 30 mL of ethanol, followed by the addition of 0.5 g of NH$_2$OH·HCl and 0.1 mL of trimethylamine. After stirring for 12 h at 75 °C, the product was collected by filtration, washed several times with deionized water, and then finally dried at 40 °C under vacuum. COFs 3-AO and 4-AO were synthesized via a similar synthetic route, using COF 3 and COF 4, respectively.

Synthesis of COFs 3-Pd-AO and 4-Pd-AO

For the synthesis of COF 3-Pd-AO, 0.1 g of COF 3 was dispersed in 100 mL of acetonitrile, followed by the addition of 63.5 mg of [PdCl$_2$(CH$_2$CN)$_2$]. After heating at 65 °C for 24 h, the product was collected by filtration, washed several times with acetonitrile and methanol, and then finally dried under vacuum to yield COF 3-Pd. Subsequently, COF 3-Pd-AO was obtained by following the above procedure. COF 4-Pd-AO was synthesized via a similar synthetic route, using COF 4 as the starting material.

Results and Discussion

Synthesis and characterization of the COF adsorption–photocatalysts

To render COFs with specific functionality as uranium extraction materials, our initial step was to synthesize a three-component COF with one-dimensional (1D) channels. This was achieved via the Schiff-base condensation of Pa, Tp, and Bpy under solvothermal conditions (denoted as COF 1) (Figure 2a). The chemical structure of COF 1 was determined by Fourier transform infrared (FTIR) spectroscopy, solid-state cross-polarization magic angle spinning ^{13}C NMR (^{13}C CP/MAS NMR), and powder X-ray diffraction (PXRD). The disappearance of –NH$_2$ stretching bands at ~3500–3300 cm^{-1} and –CHO stretching band at ~1638 cm^{-1} in the precursors indicated the formation of imine bonds in the COF 1 structure (Supporting Information Figures S1 and S2). The solid-state ^{13}C CP/MAS NMR spectrum of the product further showed the characteristic signal for the C–NH group at 159.6 ppm (Supporting Information Figure S6). A possible theoretical crystalline structural simulation of COF 1 was determined by Materials Studio Software,[47] built under a monoclinic
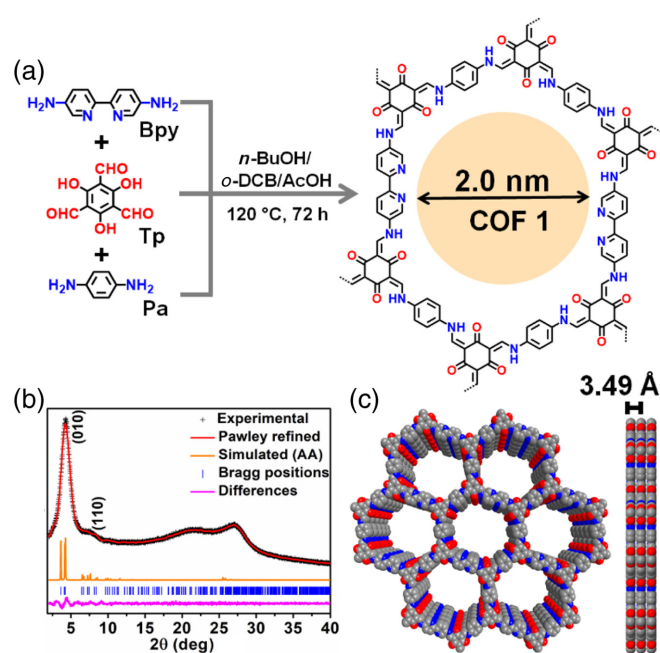
Figure 2 | *Preparation and characterization of COF 1. (a) Synthetic scheme of COF 1 through the condensation of Bpy, Tp, and Pa. (b) Experimental and simulated PXRD patterns of COF 1. (c) Top and side view of the eclipsed (AA) stacking crystal structure of COF 1. Hydrogen atoms are omitted for clarity. The C, N, and O atoms are represented by gray, blue, and red spheres, respectively.*

P21/m space group with unit cell parameters of a = 27.60 Å, b = 26.78 Å, and c = 3.54 Å, α = β = 90°, and γ = 128.02° (Supporting Information Tables S1 and S2). Comparing the eclipsed stacking (AA) and staggered stacking (AB) modes showed the experimental data more closely matched the calculated AA stacking mode with an unweighted-profile R factor (R_p) = 1.76% and weighted-profile R factor (R_{wp}) = 2.34%, suggesting the validity of the computational model (Figure 2b and Supporting Information Table S2). The PXRD pattern of COF 1 showed diffraction peaks at 4.26° and 7.61°, which could readily be assigned to the (010) and (110) Bragg peaks of the P21/m structure, respectively (Figure 2b). Based on these results, we deduced that COF 1 demonstrated a two-dimensional (2D) structure when viewed from the top with hexagonal 1D channels with a theoretical pore size of 2.0 nm (Figures 2a and 2c). The side view showed the layered stacking structure with an interlayer distance of 3.49 Å. Thermogravimetric analysis (TGA) demonstrated that COF 1 was thermally stable up to 450 °C under a nitrogen atmosphere (Supporting Information Figure S15).

Considering the selective uranyl recognition and coordination abilities of amidoxime groups, we sought to replace the Pa linker in COF 1 with an amidoxime-rich linker to produce the amidoxime functionalized COFs. Based on our previous experience, amidoxime functional

groups can be produced by hydrolysis of cyano groups with hydroxylamine. Based on this approach, a cyano-functionalized COF was first prepared by combining Db, Tp, and Bpy, finally producing COF 2 with a monoclinic unit cell with a = 27.25 Å, b = 26.84 Å, and c = 3.53 Å, α = β = 90°, and γ = 129.15° (Figure 3a, route A, Supporting Information Tables S1 and S3). The experimental PXRD pattern closely matched the calculated results based on a model with eclipsed AA stacking (Figure 3b). The sharp peaks observed at 3.98° and 7.76° in the PXRD pattern of COF 2 correspond to the (100) and (110) planes, respectively. The observed peaks at 95.1 ppm and 2219 cm^{-1} in the solid-state ^{13}C NMR and FTIR spectra, respectively, confirmed the presence of cyano groups (–C≡N) in the structure (Figure 3d and Supporting Information Figure S7). The characterization results and calculated unit cell for COF 2 (Figure 3c) revealed a structure similar to COF 1. However, due to the introduction of cyano groups, COF 2 possessed a smaller pore size of ~1.9 nm. COF 3, another nitrile-functionalized framework, was synthesized with the same general synthetic strategy, using combinations of Bpdba, Tp, and Bpy (Figure 3a, route B). FTIR, solid-state ^{13}C CP/MAS NMR, and PXRD analysis were used to establish the probable structure of COF 3 (2D eclipsed AA stacking, with hexagonal 1D channels approximately 2.6 nm in diameter) (Figures 3f and 3g and Supporting Information Figure S8 and Tables S1 and S4). TGA analysis showed COF 2 and COF 3 were stable up to 450 °C and 400 °C, respectively, by heating under N$_2$ (Supporting Information Figures S16 and S17). Chemical transformation of the cyano groups in these COFs into amidoxime groups with hydroxylamine in ethanol produced COF 2-AO and COF 3-AO, respectively (Figures 3a, 3e, and 3i). The absence of a nitrile stretch (~2219 cm^{-1}) in the FTIR spectra of COF 2-AO and COF 3-AO accords well with the successful modification of cyano groups to amidoxime groups (Figures 3d and 3h). Solid-state ^{13}C NMR analyses further confirmed this transformation, evidenced by the disappearance of the cyano groups peak at 95.1 (COF 2) and 97.5 ppm (COF 3) and the emergence of C=N signals (from amidoxime groups) at 166.7 and 160.5 ppm from the generated amidoxime groups in the spectra of COF 2-AO and COF 3-AO, respectively (Supporting Information Figures S7 and S8). PXRD patterns showed the parent structures were retained after the amidoxime functionalization (Figures 3b and 3f).

Aside from acting simply as uranyl adsorbents, COF materials are able to act as photocatalysts for the reductive deposition of uranyl as solid products, such as UO$_2$, thereby offering a practical technology for uranium extraction and collection.[31] This inspired us to construct an adsorption–photocatalysis COF system to achieve efficient uranium extraction from seawater. Triazine[48–51] and [Pd(ligand)$_x$Cl$_2$][46,52,53] components are commonly used as photosensitizing agents in the literature. Accordingly, we aimed to install both of these photosensitizing groups
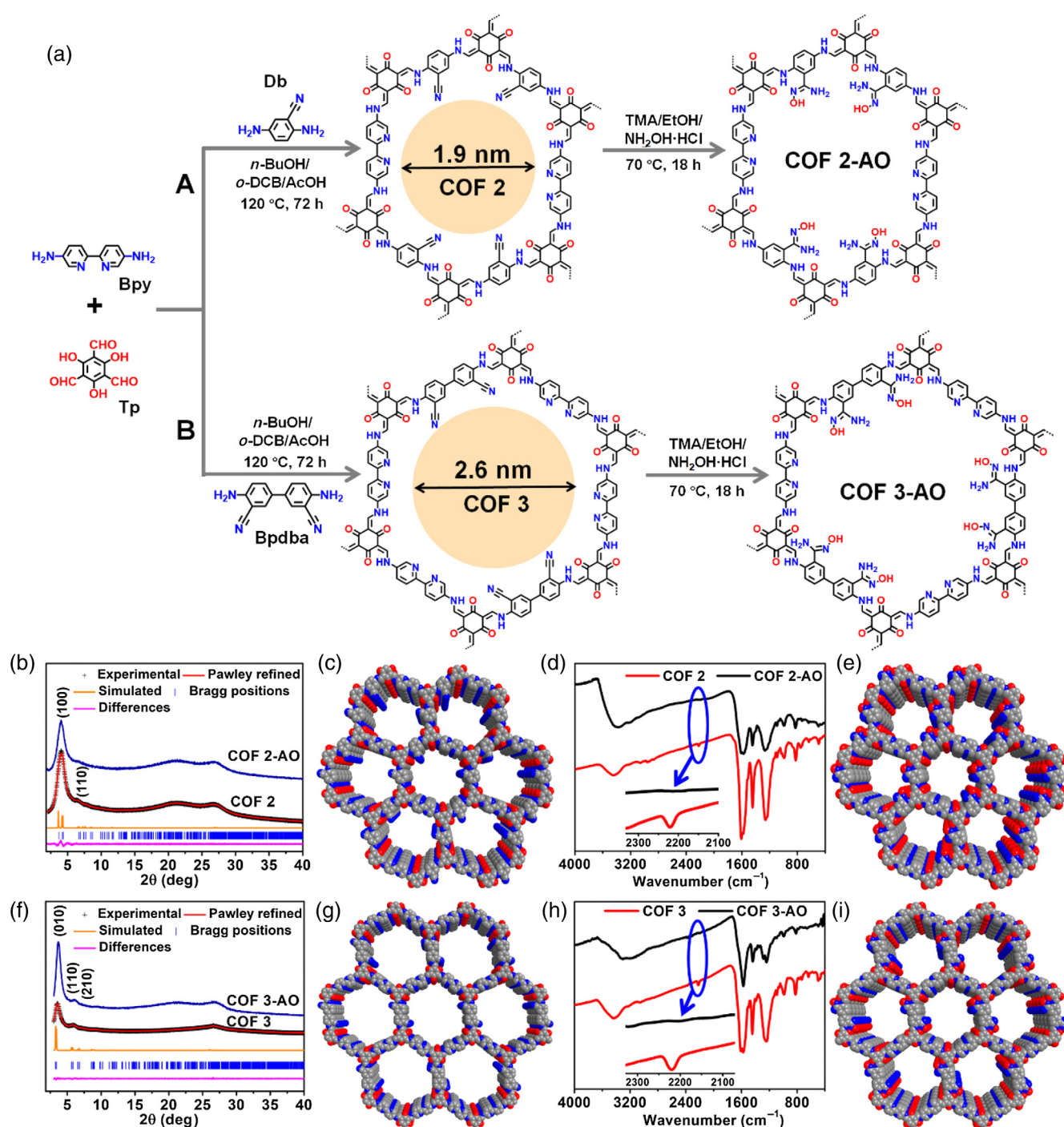
Figure 3 | *Preparation and characterization of COFs 2, 3, 2-AO, 3-AO. (a) Synthetic schemes of COF 2 and COF 3, and their corresponding post-synthetic modification to chemically transformation cyano groups to amidoxime groups, yielding COF 2-AO, and COF 3-AO, respectively. (b) Experimental and simulated PXRD profiles. (c) Graphic view of the eclipsed AA stacking structure of COF 2. (d) FTIR spectra of COF 2 and COF 2-AO. (e) Graphic view of COF 2-AO. (f) Experimental and simulated PXRD profiles. (g) Graphic view of COF 3. (h) FTIR spectra of COF 3 and COF 3-AO. (i) Graphic view of COF 3-AO. Hydrogen atoms are omitted for clarity. The C, N, and O atoms are represented by gray, blue, and red spheres, respectively.*

into a COF framework. To achieve this, as schematically illustrated in Figure 4a, a triazine containing molecule TATTA was used instead of Tp in the COF 3 synthesis.

This produced COF 4. The structure of COF 4 was determined from PXRD measurements in conjunction with structural calculations and Pawley refinements using
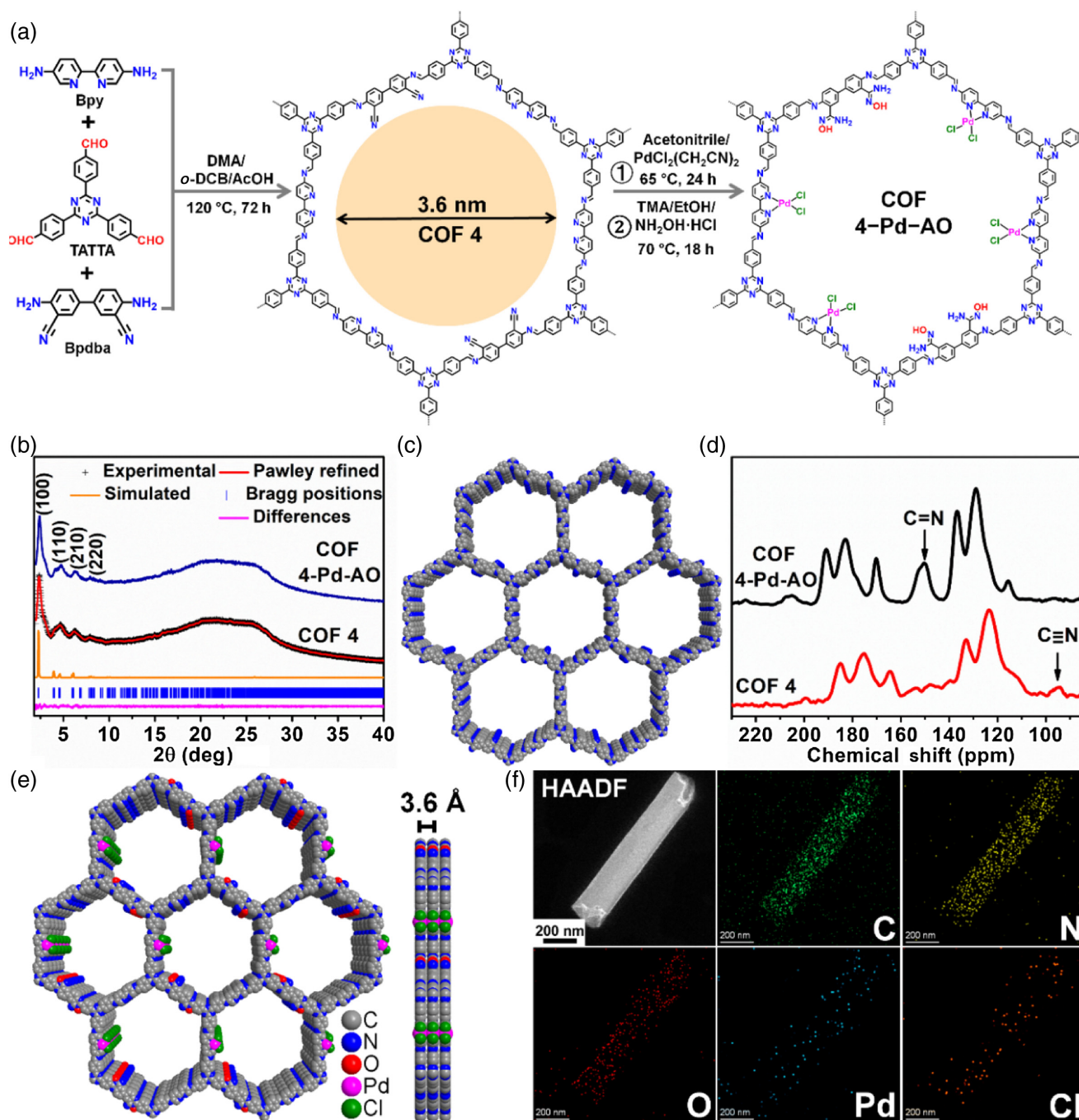
Figure 4 | *Preparation and characterizations of COF 4 and COF 4-Pd-AO. (a) Synthetic scheme of COF 4 and corresponding post-synthetically modified COF 4-Pd-AO. (b) Experimental and simulated PXRD profiles. (c) Graphic view of the eclipsed AA stacking structure of COF 4. (d) Solid-state ^{13}C CP/MAS NMR spectra of COF 4 and COF 4-Pd-AO. (e) Top and side view of COF 4-Pd-AO. (f) HAADF-STEM and corresponding elemental mapping images of COF 4-Pd-AO. Hydrogen atoms are omitted for clarity. The C, N, O, Pd, and Cl atoms are represented by gray, blue, red, magenta, and olive spheres, respectively.*

Materials Studio Software.[47] The experimental data were a close match for the calculated data (negligible difference, R_p, 1.21%; R_{wp}, 1.84%), indicating phase purity of COF 4 and an AA stacking mode (Figures 4b and 4c and Supporting Information Tables S1 and S5). The compound possesses a

2D layer structure with 3.6 nm honeycomb-like open channels (Figures 4a and 4c). FTIR spectroscopy showed characteristic peaks at 2219 and 1619 cm^{-1}, confirming the presence of cyano groups and imine C=N bonds, respectively, in the COF 4 structure (Supporting Information

Figure S4). The ^{13}C CP/MAS NMR showed a peak at 94.6 ppm attributed to C≡N (Figure 4d). TGA showed that COF 4 possesses very high thermal stability up to 500 °C in N_2 (Supporting Information Figure S18). The obtained COF was then stirred with [$PdCl_2(CH_2CN)_2$] in acetonitrile to produce a Pd(II)-functionalized material. A final amidoximation process with hydroxylamine yielded COF 4-Pd-AO, with the amidoxime groups located in large pores (Figures 4a, 4b, 4d, and 4e). PXRD confirmed a high crystallinity was retained after the functionalization steps (Figure 4b). High-angle annular dark-field scanning transmission electron microscopy (HAADF-STEM) and corresponding elemental mapping images together with X-ray photoelectron spectroscopy (XPS) indicated that Pd and Cl were successfully incorporated into the COF framework (Figure 4f and Supporting Information Figures S20, S28–S30). Pd $3d_{5/2}$ and Pd $3d_{3/2}$ XPS peaks were observed at 338.4 and 343.8 eV, respectively, consistent with literature values reported for palladium in bipyridine-Pd(II) structures.[53]

To validate the utility of COF 4-Pd-AO as a high-performance adsorption–photocatalyst for uranyl adsorption and photocatalytic U(VI) reduction-deposition, we also synthesized several reference materials (COF 3-Pd-AO and COF 4-AO). The detailed synthetic procedures and characterizations of these additional COFs are provided in Supporting Information Figures S3, S5, S9, S10, and S19.

Porosity, chemical stability, and photoelectric properties

First, the stabilities of the various synthesized multicomponent COFs were studied under different harsh conditions. After 24 h of immersion in HCl (pH 3), NaOH (pH 12), and natural seawater, the COFs remained intact with no framework collapse or undesirable phase transitions occurring, as evidenced by the PXRD patterns of the treated COFs being the same with the as-prepared COFs (Figure 5a and Supporting Information Figures S11–S14). Nitrogen adsorption–desorption isotherms were measured at 77 K to evaluate the surface areas and porosities of the multicomponent COFs. The isotherms showed large N_2 uptakes at P/P_O values below 0.1, and a more gradual uptake at a pressure between 0.1 to 0.95 (P/P_O), indicating that both micropores and small mesopores were present in the COFs, consistent with their crystal structures (Figure 5b and Supporting Information Figures S21, S23, S25). The Brunauer–Emmett–Teller (BET) surface areas and pore size distributions of the COFs are summarized in Supporting Information Table S6 and Figures S21–S27. The BET surface area calculated for COF 4-Pd-AO was 989 m^2/g, lower than that of COF 4-AO (1094 m^2/g) and COF 4 (1932 m^2/g), demonstrating the retention of significant porosity after $PdCl_2$ functionalization. The as-synthesized COFs were next characterized by UV–vis

spectroscopy in diffuse reflectance mode to determine their optical properties. The spectra for COFs 4, 4-AO, 4-Pd-AO, and 3-Pd-AO showed strong absorption bands in the visible region with absorption onsets ranging from 520 nm to 600 nm (Supporting Information Figure S31). The optical band gaps were estimated to be 2.10, 2.19, 1.89, and 2.00 eV for COFs 4, 4-AO 4-Pd-AO, and 3-Pd-AO, respectively (Figure 5c). COF 4-Pd-AO showed the lowest band gap, indicating it needed the least energy to achieve an effective separation of charge carriers. The internal resistances of the COFs were evaluated by electrochemical impedance spectroscopy (EIS) analysis. COF 4-Pd-AO displayed a smaller semicircular diameter in EIS Nyquist curves compared with COFs 4, 4-AO, and 3-Pd-AO, indicating a smaller interfacial charge-transfer resistance (Figure 5d). Moreover, the conduction-band position of each COF was estimated by measuring the flat band potential (E_{fb}) via Mott–Schottky plots. COF 4-Pd-AO exhibited a negative E_{fb} of −1.04 V versus a Ag/AgCl electrode, much lower than that of COFs 4 (−0.57 V), 4-AO (−0.6 V), and 3-Pd-AO (−0.52 V) (Figure 5e). The positive slopes in Figure 5e suggest these COFs are n-type semiconductors. Generally, the conduction band (CB) of n-type semiconductors is equal to the flat band potential.[54] Using the results of the flat band potential measurements and the optical band gaps, the positions of the CBs and valence bands (VBs) in the different COFs were estimated: COFs 4 (CB = −0.37 eV, VB = 1.73 eV), COF 4-AO (CB = −0.40 eV, VB = 1.79 eV), COF 4-Pd-AO (CB = −0.84 eV, VB = 1.05 eV), and COF 3-Pd-AO (CB = −0.32 eV, VB = 1.68 eV) (Figure 5f). The photocurrent density curves for COF 3-Pd-AO and COF 4-Pd-AO showed that photogenerated charges were created under visible light irradiation, thus validating our strategy to introduce photoactive components in the COFs (Supporting Information Figure S32). The photoresponse for COF 4-Pd-AO was larger than that for 3-Pd-AO, which is explained by the former containing triazine and bipyridyl-Pd(II) sensitizers, whereas the latter only contained bipyridyl-Pd(II) moieties. Obviously, the CB positions of the COFs satisfy the requirement for U(VI) reduction to U(IV) [0.411 V vs normal hydrogen electrode (NHE)], suggesting these COFs could be utilized as an effective adsorption–photocatalyst platform for uranium extraction from seawater.[55]

The characterization studies above revealed the successful synthesis of a series of multicomponent COFs, with COF 4-Pd-AO possessing all of the following advantages: (1) excellent stability in acid, basic, and seawater media; (2) imine bonds, amidoxime groups, and [Pd(bpy)$_2$Cl$_2$] groups that imparted hydrophilicity to the COF; (3) abundant amidoxime groups as uranyl-binding sites; (4) triazine functional groups providing photocatalytic activity; (5) bipyridine-Pd(II) sites as secondary photosensitizing sites to boost photocatalytic performance. As a proof-of-concept, we next conducted a
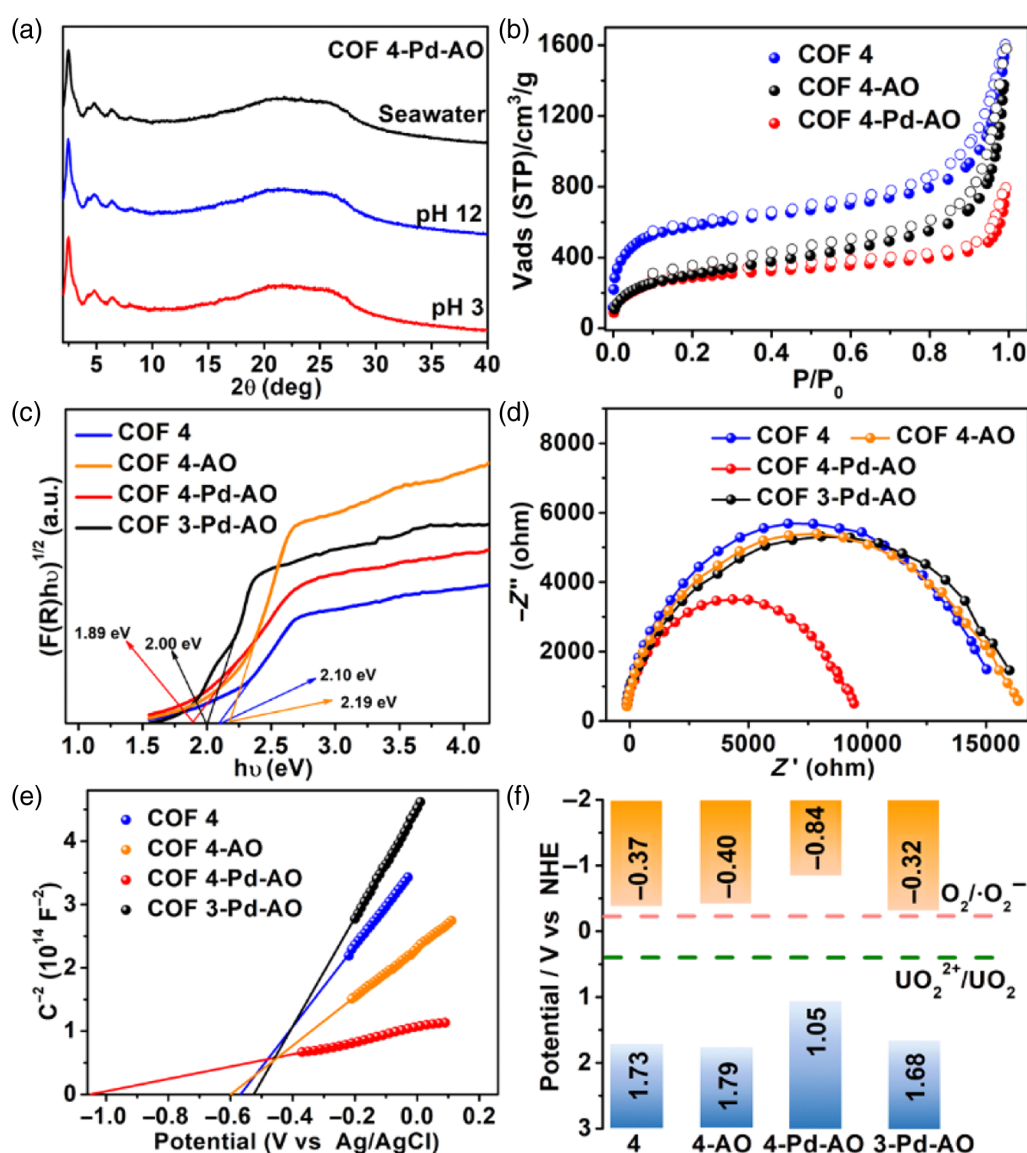
Figure 5 | *Characterization of synthesized COFs. (a) PXRD patterns of COF 4-Pd-AO after treatment under different conditions. (b) N_2 sorption isotherms measured at 77 K for COFs 4, 4-AO, and 4-Pd-AO. (c) Estimated band gap of COFs 4, 4-AO, 4-Pd–AO, and 3–Pd–AO. (d) Electrochemical impedance spectra (EIS) of COFs 4, 4–AO, 4–Pd-AO, and 3-Pd-AO. (e) Mott–Schottky plots for COFs 4, 4-AO, 4-Pd-AO, and 3-Pd-AO. (f) Band alignment of COFs 4, 4-AO, 4-Pd-AO, and 3-Pd-AO.*

series of experiments to assess the uranium extraction performance of the various multicomponent COFs we had synthesized.

Physicochemical adsorption studies

The uranyl adsorption properties of the different COF materials were initially studied in spiked-seawater solutions at pH 8.1. Equilibrium adsorption capacities were determined by varying the concentrations of uranium from 0 to ~20 ppm at a fixed sorbent concentration of 0.05 mg/mL. After adsorption equilibrium was attained, the tested capacity per gram of sorbent for COFs 4-AO,

4-Pd-AO, 3-AO, 3-Pd-AO, and 2-AO, were 155.7, 150.8, 146.7, 134.4, and 63.2 mg/g, respectively (Figure 6a and Supporting Information Figures S33 and S34). COFs 4-AO and 4-Pd-AO (as well as COFs 3-AO and 3-Pd-AO) exhibited similar capacities, suggesting the coordinated Pd(II) did not block any uranyl adsorption sites. The equilibrium adsorption data were fitted well by a Langmuir model with correlation coefficients (Supporting Information Figures S33 and S34 and Table S7). The amidoxime functionalized COFs 4-AO, 4-Pd-AO, 3-AO, 3-Pd-AO, and 2-AO showed rapid adsorption rates for uranyl (Figure 6b and Supporting Information Figures S35 and S36 and Table S8), suggesting that the
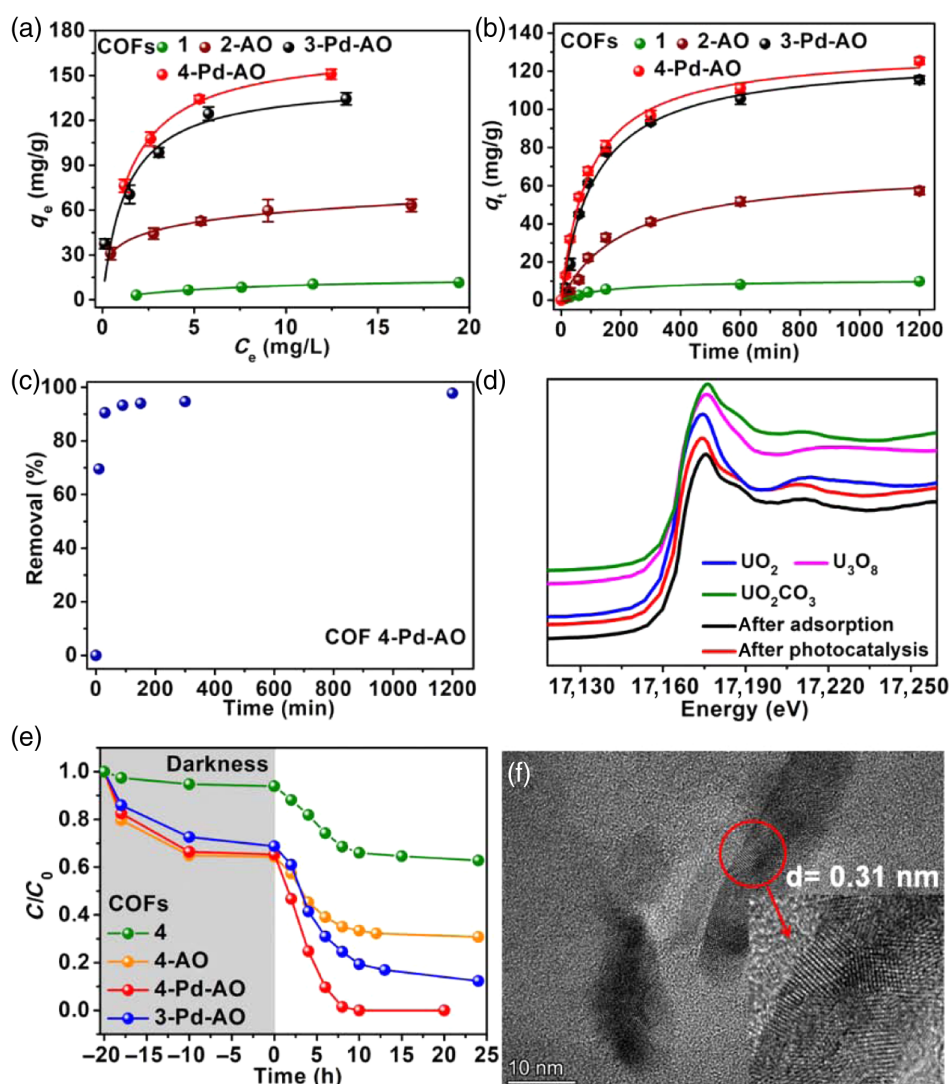
Figure 6 | *Uranium adsorption isotherms, kinetics, XANES, and TEM results. (a) Equilibrium adsorption isotherms for uranyl adsorption on different materials at a fixed adsorbent concentration of 0.05 mg/mL in uranyl-spiked seawater (uranium concentration from 0 to ~20 ppm; the lines fit with the Langmuir model). (b, c) Uranyl adsorption kinetics on different materials at an initial uranium concentration of ~9 ppm and ~25 ppb in uranyl-spiked seawater, respectively. (d) U L_{III}-edge XANES spectra for COF 4-Pd-AO after uranium extraction studies. UO_2, U_3O_8, and UO_2CO_3 are employed for comparison. (e) Uranium extraction from spiked seawater with initial uranium concentrations of ~20 ppm, using COFs 4, 4-AO, 4-Pd-AO, and 3-Pd-AO as adsorbent–photocatalysts. (f) HRTEM image of COF 4-Pd-AO (attached solid nanoparticle) after adsorption–photocatalysis study. The data for UO_2 stand in 6d were reported in our previous work.[8]*

hierarchical pore structures and amidoxime chelating groups allowed rapid pore penetration by uranyl and subsequently strong binding, respectively. It is worth noting that COF 4-Pd-AO possessed extremely rapid uranyl capture abilities in a ~25 ppb spiked-seawater sample, with 90% and 94% uranyl removal achieved within 30 and 90 min, respectively (Figure 6c). In comparison, COF 1 offered a poor uranyl adsorption capacity and slow kinetics, which confirmed the key role of amidoxime chelating groups in selective uranyl capture (Figures 6a and 6b). In addition, equilibrium uranium uptake capacity was further

determined by varying the initial uranium concentrations from ~50 to ~800 ppm (without pH adjustment). As expected, 3-Pd-AO and 4-Pd-AO showed similar experimental and theoretical uptake capacities, respectively, again confirming the strong uranyl-affinities of amidoxime groups in these COFs (Supporting Information Figure S37 and Table S9). X-ray absorption near edge structure (XANES) and X-ray absorption fine structure (EXAFS) data collected at U L_{III} edge was employed to study the coordination environments and valence state of uranium in functionalized COF materials after the uranyl

adsorption tests. XANES spectra revealed a pre-edge peak for COF 4-Pd-AO, similar to that observed for UO_2CO_3, suggesting the uranium existed in the form of adsorbed uranyl, that is, U(VI) (Figure 6d). The EXAFS R-space (and k-space) plot and fitting results suggested the U(VI) coordination environment was consistent with a uranyl-benzamidoxime η^2 binding motif model (Supporting Information Figures S38–S40 and Table S10).[22,34,56]

Adsorption–photocatalytic uranium extraction studies

Having examined the uranyl adsorption properties of the various COFs, attention was then placed on examining the adsorption–photocatalytic reduction properties of COFs 4, 4-AO, 4-Pd-AO, and 3-Pd-AO in uranyl-spiked seawater (~20 ppm uranium based) at pH 8.1 and natural seawater. Before turning on the xenon lamp fitted with a 420 nm cutoff filter, the dispersions were stirred in the dark at room temperature over 20 h to allow uranyl adsorption to be established. After 8 h of light irradiation, COFs 4, 4-AO, 3-Pd-AO, and 4-Pd-AO were determined to have uranium removal efficiencies of approximately 31.4%, 65.0%, 75.5%, and >98.6%, respectively (Figure 6e). COF 4-Pd-AO achieved a removal efficiency >99.9% after 10 h, which is 33.4% higher than that of COF 4-AO, confirming the superior performance of COF 4-Pd-AO and the important role of the bipyridyl-Pd(II) groups in boosting the photocatalytic activity. The uranium adsorption–photocatalytic performance of COF 4-Pd-AO was retained with negligible loss in capacity after six cycles, suggesting good reusability (Supporting Information Figure S41). PXRD and FTIR revealed the structure was retained after cycling tests (Supporting Information Figures S42 and S43). The Pd 3d XPS spectrum of the catalyst after catalysis was identical to those of the positively charged Pd(II) indicating the stability of the bipyridine-Pd(II) structures under catalytic conditions (Supporting Information Figure S44). Importantly, through the introduction of photocatalytic function in the COFs, much better extraction performance was realized compared to COFs employing only physicochemical adsorption of uranyl. We carried out the XANES, XPS, and transmission electron microscopy (TEM) measurements to analyze the solid product produced by COF 4-Pd-AO during the adsorption–photocatalytic experiment. The XANES spectrum at the U L_{III}-edge was similar to that of UO_2, indicating the presence of U(IV) as the dominant oxidation state (Figure 6d).[57] The U 4f XPS spectrum for the product confirmed the presence of U(IV) again, consistent with the presence of a UO_2 product (Supporting Information Figure S45).[31,57] An amount of U(VI) was also detected, possibly resulting from surface oxidation of UO_2 in the air or alternatively some non-reduced uranyl. STEM and corresponding element mapping images showed that U and O are homogeneously attached through the COF material (Supporting Infor-

mation Figure S46). The high-resolution TEM (HRTEM) image taken from an attached solid nanoparticle showed lattice fringes with a spacing of 0.31 nm, corresponding to the interlayer spacing between (111) planes in cubic UO_2 (Figure 6f and Supporting Information Figure S47).

Extraction of uranium from natural seawater

Encouraged by the aforementioned results, we next carried out experiments to determine the ability of COF 4-Pd-AO to extract uranium from natural seawater. 4-Pd-AO (10 mg) was spread on the top of the column filled with sea sand, and natural seawater was cycled through the column from top to bottom (Supporting Information Figure S48). COF 4-Pd-AO exhibited excellent uranium extraction performance, with a calculated uranium uptake of 4.62 mg/g per day from natural seawater under visible light irradiation, validating the excellent performance of COF 4-Pd-AO for selective uranium extraction from seawater. Our novel adsorption–photocatalytic strategy using COF 4-Pd-AO exhibited superior or comparable performance to other state-of-the-art materials or technologies for uranium extraction from seawater (Supporting Information Table S11), thus showing great promise for practical applications.

Photocatalytic mechanism and antibiofouling activity studies

To better understand the photocatalytic properties of COF 4-Pd-AO containing triazine and bipyridine-metal photoactive groups, electron spin resonance spectroscopy (ESR) studies were carried out to investigate the types of active oxygen radical species generated by the photocatalyst under visible light irradiation. Sharp ESR signals were observed after adding 3,4-dihydro-2,3-dimethyl-2H-pyrrole 1-oxide (DMPO) and 2,2,6,6-tetramethylpiperidine (TEMP) as trapping agents, indicating the generation of superoxide radicals ($O_2^{\bullet-}$) and singlet oxygen ($^1O_2$), respectively. No ESR signal due to trapped hydroxyl radicals ($\bullet$OH) was detected (Figure 7a). These results demonstrated that under visible light irradiation, COF 4-Pd-AO generates $O_2^{\bullet-}$ and $^1O_2$ in the presence of dissolved O_2, thus imparting the COF with marine antifouling properties in the seawater. CB electrons not consumed in the reduction of U(VI) to U(IV) (i.e., uranyl conversion to UO_2) are thus used to generate $O_2^{\bullet-}$. Antibacterial studies further confirmed our proposition. In contrast to control experiments conducted in the dark, marine bacteria growth was strongly suppressed in the presence of COF 4-Pd-AO under light irradiation, consistent with the generated $O_2^{\bullet-}$ and $^1O_2$ damaging the cell wall of the bacteria (Figures 7b–7d). Supporting Information Table S12 showed that a high inhibition rate of 96.86% was achieved with COF 4-Pd-AO under visible light irradiation in natural seawater. In addition, COF 4-Pd-AO exhibited high inhibition rates of 66.48% and
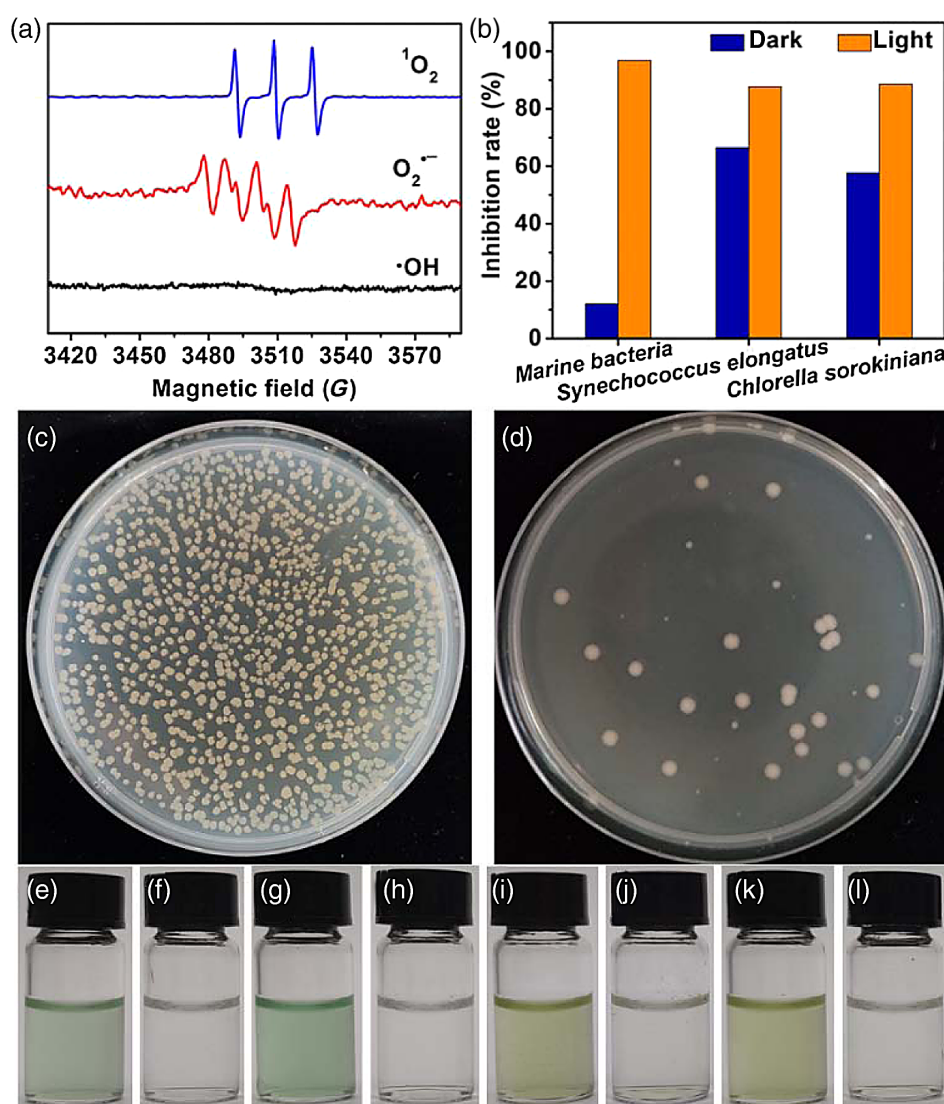
Figure 7 | *ESR analysis and antibiofouling activity of COF 4-Pd-AO. (a) ESR spectra for $O_2^{\bullet-}$-DMPO and $^1O_2$-TEMP complexes formed by visible light irradiation of COF 4-Pd-AO. (b) Antibiofouling spectrum of COF 4-Pd-AO. Photographs of marine bacteria colonies after treatment with COF 4-Pd-AO in (c) the dark and (d) under visible light conditions. Photographs of* Synechococcus elongatus *under dark (e) and visible light (g) without catalyst. Photographs of* Synechococcus elongatus *treated with COF 4-Pd-AO under dark (f) and visible light (h). Photographs of* Chlorella sorokiniana *under dark (i) and visible light (k) without catalyst. Photographs of* Chlorella sorokiniana *treated with COF 4-Pd-AO under dark (j) and visible light (l).*

57.65% towards algae *Synechococcus elongates* and *Chlorella sorokiniana*, respectively, under dark conditions. Notably, the inhibition rates of COF 4-Pd-AO can be improved under visible light irradiations, thus demonstrating impressive broad-spectrum biofouling resistance under experimental conditions (Figures 7b and 7e–7l and Supporting Information Table S12). Taken together, these results show that COF 4-Pd-AO can effectively extract uranium from seawater as UO_2 under visible light, whilst also displaying potent antibiofouling properties against marine bacteria and marine algae.

Based on the detailed experimental investigations above, COF 4-Pd-AO emerges as a very promising adsorbent–photocatalyst for uranium extraction from seawater. The rational introduction of functional linkers bearing amidoxime functional groups boosted COF surface hydrophilicity and enhanced uranyl uptake, whilst the triazine and bipyridine-Pd(II) sites photocatalytically reduced the adsorbed U(VI) to $U(IV)O_2$ by transferring two electrons, with the latter being easily collected. Its remarkable resistance against biofouling allowed COF 4-Pd-AO to be durably recycled for further use. Results

of this work will encourage the development of other COF-based adsorption–photocatalytic systems for selective metal capture from seawater, leveraging rational multicomponent COF design, synthesis, and functionalization.

Conclusion

A multicomponent covalent-organic framework (COF 4-Pd-AO) was successfully developed as a new type of adsorption–photocatalyst for uranium extraction from seawater. Control experiments with related COFs, missing one or more of the characteristic components of COF 4-Pd-AO, revealed that the uranium extraction performance of multicomponent COFs can be progressively tuned through linker modification. COF 4-Pd-AO benefitted from a well-defined pore structure, linkers exposing a high density of amidoxime chelating groups for uranyl binding, and two types of photocatalytically active sites for the reduction of adsorbed uranyl to UO_2, thereby enabling efficient adsorption–photocatalytic extraction of uranium from seawater (uranium extraction performance as high as 4.62 mg/g per day in natural seawater). Reactive oxygen species, including superoxide radicals and singlet oxygen, generated by COF 4-Pd-AO under visible light irradiation served to prevent biofouling, enhancing the practicality of the adsorption–photocatalytic system for real-world uranium extraction from seawater. Further studies aimed at increasing the uranyl adsorption capacity and changing the end products of COF-based materials for uranium extraction from seawater are ongoing in our laboratory.

Supporting Information

Supporting Information is available and includes additional chemicals, instrumentation, uranium extraction experimental details, crystallographic data, FTIR spectra, solid-state ^{13}C CP/MAS NMR spectra, PXRD patterns, TGA curves, XPS spectra, N_2 sorption and pore size analysis, HAADF-TEM images, energy-dispersive X-ray spectroscopy (EDS) spectra, UV–vis spectra, photocurrent curves, uranium adsorption data and fitting results, and X-ray absorption spectroscopy (XAS) fitting results.

Conflict of Interest

There is no conflict of interest to report.

Acknowledgments

References

1. Adamantiades, A.; Kessides, I. Nuclear Power for Sustainable Development: Current Status and Future Prospects. *Energy Policy* **2009**, *37*, 5149–5166.

2. Mayer, K.; Wallenius, M.; Lutzenkirchen, K.; Horta, J.; Nicholl, A.; Rasmussen, G.; van Belle, P.; Varga, Z.; Buda, R.; Erdmann, N.; Kratz, J. V.; Trautmann, N.; Fifield, L. K.; Tims, S. G.; Frohlich, M. B.; Steier, P. Uranium from German Nuclear Power Projects of the 1940s-A Nuclear Forensic Investigation. *Angew. Chem. Int. Ed.* **2015**, *54*, 13452–13456.

3. Sholl, D. S.; Lively, R. P. Seven Chemical Separations to Change the World. *Nature* **2016**, *532*, 435–437.

4. Kim, J.; Tsouris, C.; Mayes, R. T.; Oyola, Y.; Saito, T.; Janke, C. J.; Dai, S.; Schneider, E.; Sachde, D. Recovery of Uranium from Seawater: A Review of Current Status and Future Research Needs. *Sep. Sci. Technol.* **2013**, *48*, 367–387.

5. Lindner, H.; Schneider, E. Review of Cost Estimates for Uranium Recovery from Seawater. *Energy Econ.* **2015**, *49*, 9–22.

6. Abney, C. W.; Mayes, R. T.; Saito, T.; Dai, S. Materials for the Recovery of Uranium from Seawater. *Chem. Rev.* **2017**, *117*, 13935–14013.

7. Shao, D.; Hou, G.; Li, J.; Wen, T.; Ren, X.; Wang, X. PANI/GO as a Super Adsorbent for the Selective Adsorption of Uranium(VI). *Chem. Eng. J.* **2014**, *255*, 604–612.

8. Yang, H.; Liu, X.; Hao, M.; Xie, Y.; Wang, X.; Tian, H.; Waterhouse, G. I. N.; Kruger, P. E.; Telfer, S. G.; Ma, S. Functionalized Iron-Nitrogen-Carbon Electrocatalyst Provides a Reversible Electron Transfer Platform for Efficient Uranium Extraction from Seawater. *Adv. Mater.* **2021**, *33*, 2106621.

9. Liu, C.; Hsu, P.-C.; Xie, J.; Zhao, J.; Wu, T.; Wang, H.; Liu, W.; Zhang, J.; Chu, S.; Cui, Y. A Half-Wave Rectified Alternating Current Electrochemical Method for Uranium Extraction from Seawater. *Nat. Energy* **2017**, *2*, 17007.

10. Ismail, A. F.; Yim, M.-S. Investigation of Activated Carbon Adsorbent Electrode for Electrosorption-Based Uranium Extraction from Seawater. *Nucl. Eng. Technol.* **2015**, *47*, 579–587.

11. Wang, F.; Li, H.; Liu, Q.; Li, Z.; Li, R.; Zhang, H.; Liu, L.; Emelchenko, G. A.; Wang, J. A Graphene Oxide/Amidoxime Hydrogel for Enhanced Uranium Capture. *Sci. Rep.* **2016**, *6*, 19367.

12. Yue, Y.; Sun, X.; Mayes, R. T.; Kim, J.; Fulvio, P. F.; Qiao, Z.; Brown, S.; Tsouris, C.; Oyola, Y.; Dai, S. Polymer-Coated Nanoporous Carbons for Trace Seawater Uranium Adsorption. *Sci. China Chem.* **2013**, *56*, 1510–1515.

13. Lebed, P. J.; Savoie, J.-D.; Florek, J.; Bilodeau, F.; Larivière, D.; Kleitz, F. Large Pore Mesostructured

Organosilica-Phosphonate Hybrids as Highly Efficient and Regenerable Sorbents for Uranium Sequestration. *Chem. Mater.* **2012**, *24*, 4166–4176.

14.   Feng, M. L.; Sarma, D.; Qi, X. H.; Du, K. Z.; Huang, X. Y.; Kanatzidis, M. G. Efficient Removal and Recovery of Uranium by a Layered Organic-Inorganic Hybrid Thiostannate. *J. Am. Chem. Soc.* **2016**, *138*, 12578–12585.

15.   Yue, Y.; Mayes, R. T.; Kim, J.; Fulvio, P. F.; Sun, X. G.; Tsouris, C.; Chen, J.; Brown, S.; Dai, S. Seawater Uranium Sorbents: Preparation from a Mesoporous Copolymer Initiator by Atom-Transfer Radical Polymerization. *Angew. Chem. Int. Ed.* **2013**, *52*, 13458–13462.

16.   Das, S.; Brown, S.; Mayes, R. T.; Janke, C. J.; Tsouris, C.; Kuo, L. J.; Gill, G.; Dai, S. Novel Poly(imide dioxime) Sorbents: Development and Testing for Enhanced Extraction of Uranium from Natural Seawater. *Chem. Eng. J.* **2016**, *298*, 125–135.

17.   Pan, H.-B.; Kuo, L.-J.; Wood, J.; Strivens, J.; Gill, G. A.; Janke, C. J.; Wai, C. M. Towards Understanding KOH Conditioning of Amidoxime-Based Polymer Adsorbents for Sequestering Uranium from Seawater. *RSC Adv.* **2015**, *5*, 100715–100721.

18.   Yuan, Y.; Yang, Y.; Ma, X.; Meng, Q.; Wang, L.; Zhao, S.; Zhu, G. Molecularly Imprinted Porous Aromatic Frameworks and Their Composite Components for Selective Extraction of Uranium Ions. *Adv. Mater.* **2018**, *30*, 1706507.

19.   Alexandratos, S. D.; Zhu, X.; Florent, M.; Sellin, R. Polymer-Supported Bifunctional Amidoximes for the Sorption of Uranium from Seawater. *Ind. Eng. Chem. Res.* **2016**, *55*, 4208–4216.

20.   Kuo, L.-J.; Janke, C. J.; Wood, J. R.; Strivens, J. E.; Das, S.; Oyola, Y.; Mayes, R. T.; Gill, G. A. Characterization and Testing of Amidoxime-Based Adsorbent Materials to Extract Uranium from Natural Seawater. *Ind. Eng. Chem. Res.* **2015**, *55*, 4285–4293.

21.   Brown, S.; Yue, Y.; Kuo, L.-J.; Mehio, N.; Li, M.; Gill, G.; Tsouris, C.; Mayes, R. T.; Saito, T.; Dai, S. Uranium Adsorbent Fibers Prepared by Atom-Transfer Radical Polymerization (ATRP) from Poly(vinyl chloride)-co-chlorinated Poly(vinyl chloride) (PVC-co-CPVC) Fiber. *Ind. Eng. Chem. Res.* **2016**, *55*, 4139–4148.

22.   Sun, Q.; Zhu, L.; Aguila, B.; Thallapally, P. K.; Xu, C.; Chen, J.; Wang, S.; Rogers, D.; Ma, S. Optimizing Radionuclide Sequestration in Anion Nanotraps with Record Pertechnetate Sorption. *Nat. Commun.* **2019**, *10*, 1646.

23.   Sun, Q.; Aguila, B.; Perman, J.; Ivanov, A. S.; Bryantsev, V. S.; Earl, L. D.; Abney, C. W.; Wojtas, L.; Ma, S. Bio-Inspired Nano-Traps for Uranium Extraction from Seawater and Recovery from Nuclear Waste. *Nat. Commun.* **2018**, *9*, 1644.

24.   Sun, Q.; Song, Y.; Aguila, B.; Ivanov, A. S.; Bryantsev, V. S.; Ma, S. Spatial Engineering Direct Cooperativity between Binding Sites for Uranium Sequestration. *Adv. Sci.* **2021**, *8*, 2001573.

25.   Bai, Z.-Q.; Yuan, L.-Y.; Zhu, L.; Liu, Z.-R.; Chu, S.-Q.; Zheng, L.-R.; Zhang, J.; Chai, Z.-F.; Shi, W.-Q. Introduction of Amino Groups into Acid-Resistant MOFs for Enhanced U (VI) Sorption. *J. Mater. Chem. A* **2015**, *3*, 525–534.

26.   Liu, W.; Dai, X.; Bai, Z.; Wang, Y.; Yang, Z.; Zhang, L.; Xu, L.; Chen, L.; Li, Y.; Gui, D.; Diwu, J.; Wang, J.; Zhou, R.; Chai, Z.;

Wang, S. Highly Sensitive and Selective Uranium Detection in Natural Water Systems Using a Luminescent Mesoporous Metal-Organic Framework Equipped with Abundant Lewis Basic Sites: A Combined Batch, X-ray Absorption Spectroscopy, and First Principles Simulation Investigation. *Environ. Sci. Technol.* **2017**, *51*, 3911–3921.

27.   Zhang, J.; Zhang, H.; Liu, Q.; Song, D.; Li, R.; Liu, P.; Wang, J. Diaminomaleonitrile Functionalized Double-Shelled Hollow MIL-101 (Cr) for Selective Removal of Uranium from Simulated Seawater. *Chem. Eng. J.* **2019**, *368*, 951–958.

28.   Chen, L.; Bai, Z.; Zhu, L.; Zhang, L.; Cai, Y.; Li, Y.; Liu, W.; Wang, Y.; Chen, L.; Diwu, J.; Wang, J.; Chai, Z.; Wang, S. Ultrafast and Efficient Extraction of Uranium from Seawater Using an Amidoxime Appended Metal-Organic Framework. *ACS. Appl. Mater. Interfaces* **2017**, *9*, 32446–32451.

29.   Li, H.; Zhai, F.; Gui, D.; Wang, X.; Wu, C.; Zhang, D.; Dai, X.; Deng, H.; Su, X.; Diwu, J.; Lin, Z.; Chai, Z.; Wang, S. Powerful Uranium Extraction Strategy with Combined Ligand Complexation and Photocatalytic Reduction by Postsynthetically Modified Photoactive Metal-Organic Frameworks. *Appl. Catal., B* **2019**, *254*, 47–54.

30.   Cui, W. R.; Zhang, C. R.; Jiang, W.; Li, F. F.; Liang, R. P.; Liu, J.; Qiu, J. D. Regenerable and Stable sp^2 Carbon-Conjugated Covalent Organic Frameworks for Selective Detection and Extraction of Uranium. *Nat. Commun.* **2020**, *11*, 436.

31.   Cui, W. R.; Li, F. F.; Xu, R. H.; Zhang, C. R.; Chen, X. R.; Yan, R. H.; Liang, R. P.; Qiu, J. D. Regenerable Covalent Organic Frameworks for Photo-Enhanced Uranium Adsorption from Seawater. *Angew. Chem. Int. Ed.* **2020**, *59*, 17684–17690.

32.   Cui, W.-R.; Zhang, C.-R.; Xu, R.-H.; Chen, X.-R.; Yan, R.-H.; Jiang, W.; Liang, R.-P.; Qiu, J.-D. High-Efficiency Photoenhanced Extraction of Uranium from Natural Seawater by Olefin-Linked Covalent Organic Frameworks. *ACS ES&T Water* **2021**, *1*, 440–448.

33.   Li, Y.; Guo, X.; Li, X.; Zhang, M.; Jia, Z.; Deng, Y.; Tian, Y.; Li, S.; Ma, L. Redox-Active Two-Dimensional Covalent Organic Frameworks (COFs) for Selective Reductive Separation of Valence-Variable, Redox-Sensitive and Long-Lived Radionuclides. *Angew. Chem. Int. Ed.* **2020**, *59*, 4168–4175.

34.   Sun, Q.; Aguila, B.; Earl, L. D.; Abney, C. W.; Wojtas, L.; Thallapally, P. K.; Ma, S. Covalent Organic Frameworks as a Decorating Platform for Utilization and Affinity Enhancement of Chelating Sites for Radionuclide Sequestration. *Adv. Mater.* **2018**, *30*, 1705479.

35.   Wang, D.; Song, J.; Lin, S.; Wen, J.; Ma, C.; Yuan, Y.; Lei, M.; Wang, X.; Wang, N.; Wu, H. A Marine-Inspired Hybrid Sponge for Highly Efficient Uranium Extraction from Seawater. *Adv. Funct. Mater.* **2019**, *29*, 1901009.

36.   Li, R.; Pang, L.; Ma, H.; Liu, X.; Zhang, M.; Gao, Q.; Wang, H.; Xing, Z.; Wang, M.; Wu, G. Optimization of Molar Content of Amidoxime and Acrylic Acid in UHMWPE Fibers for Improvement of Seawater Uranium Adsorption Capacity. *J. Radioanal. Nucl. Chem.* **2016**, *311*, 1771–1779.

37.   Liu, X.; Pang, H.; Liu, X.; Li, Q.; Zhang, N.; Mao, L.; Qiu, M.; Hu, B.; Yang, H.; Wang, X. Orderly Porous Covalent Organic Frameworks-Based Materials: Superior Adsorbents for Pollutants Removal from Aqueous Solutions. *Innovation* **2021**, *2*, 100076.

38. Wang, Z.; Zhang, S.; Chen, Y.; Zhang, Z.; Ma, S. Covalent Organic Frameworks for Separation Applications. *Chem. Soc. Rev.* **2020**, *49*, 708–735.

39. Gill, G. A.; Kuo, L.-J.; Janke, C. J.; Park, J.; Jeters, R. T.; Bonheyo, G. T.; Pan, H.-B.; Wai, C.; Khangaonkar, T.; Bianucci, L.; Wood, J. R.; Warner, M. G.; Peterson, S.; Abrecht, D. G.; Mayes, R. T.; Tsouris, C.; Oyola, Y.; Strivens, J. E.; Schlafer, N. J.; Addleman, R. S.; Chouyyok, W.; Das, S.; Kim, J.; Buesseler, K.; Breier, C.; D'Alessandro, E. The Uranium from Seawater Program at the Pacific Northwest National Laboratory: Overview of Marine Testing, Adsorbent Characterization, Adsorbent Durability, Adsorbent Toxicity, and Deployment Studies. *Ind. Eng. Chem. Res.* **2016**, *55*, 4264–4277.

40. Park, J.; Gill, G. A.; Strivens, J. E.; Kuo, L.-J.; Jeters, R. T.; Avila, A.; Wood, J. R.; Schlafer, N. J.; Janke, C. J.; Miller, E. A.; Thomas, M.; Addleman, R. S.; Bonheyo, G. T. Effect of Biofouling on the Performance of Amidoxime-Based Polymeric Uranium Adsorbents. *Ind. Eng. Chem. Res.* **2016**, *55*, 4328–4338.

41. Yuan, Y.; Yu, Q.; Cao, M.; Feng, L.; Feng, S.; Liu, T.; Feng, T.; Yan, B.; Guo, Z.; Wang, N. Selective Extraction of Uranium from Seawater with Biofouling-Resistant Polymeric Peptide. *Nat. Sustain.* **2021**, *4*, 708–714.

42. Chen, W.; Wang, L.; Mo, D.; He, F.; Wen, Z.; Wu, X.; Xu, H.; Chen, L. Modulating Benzothiadiazole-Based Covalent Organic Frameworks via Halogenation for Enhanced Photocatalytic Water Splitting. *Angew. Chem. Int. Ed.* **2020**, *59*, 16902–16909.

43. Zhang, S.; Cheng, G.; Guo, L.; Wang, N.; Tan, B.; Jin, S. Strong-Base-Assisted Synthesis of a Crystalline Covalent Triazine Framework with High Hydrophilicity via Benzylamine Monomer for Photocatalytic Water Splitting. *Angew. Chem. Int. Ed.* **2020**, *59*, 6007–6014.

44. Krishnaraj, C.; Sekhar Jena, H.; Bourda, L.; Laemont, A.; Pachfule, P.; Roeser, J.; Chandran, C. V.; Borgmans, S.; Rogge, S. M. J.; Leus, K.; Stevens, C. V.; Martens, J. A.; Van Speybroeck, V.; Breynaert, E.; Thomas, A.; Van Der Voort, P. Strongly Reducing (Diarylamino)benzene-Based Covalent Organic Framework for Metal-Free Visible Light Photocatalytic H_2O_2 Generation. *J. Am. Chem. Soc.* **2020**, *142*, 20107–20116.

45. Ghosh, S.; Nakada, A.; Springer, M. A.; Kawaguchi, T.; Suzuki, K.; Kaji, H.; Baburin, I.; Kuc, A.; Heine, T.; Suzuki, H.; Abe, R.; Seki, S. Identification of Prime Factors to Maximize the Photocatalytic Hydrogen Evolution of Covalent Organic Frameworks. *J. Am. Chem. Soc.* **2020**, *142*, 9752–9762.

46. Wang, H.; Wang, H.; Wang, Z.; Tang, L.; Zeng, G.; Xu, P.; Chen, M.; Xiong, T.; Zhou, C.; Li, X.; Huang, D.; Zhu, Y.; Wang, Z.; Tang, J. Covalent Organic Framework Photocatalysts: Structures and Applications. *Chem. Soc. Rev.* **2020**, *49*, 4135–4165.

47. Akkermans, R. L. C.; Spenley, N. A.; Robertson, S. H. Monte Carlo Methods in Materials Studio. *Mol. Simul.* **2013**, *39*, 1153–1164.

48. Wei, S.; Zhang, F.; Zhang, W.; Qiang, P.; Yu, K.; Fu, X.; Wu, D.; Bi, S.; Zhang, F. Semiconducting 2D Triazine-Cored Covalent Organic Frameworks with Unsubstituted Olefin Linkages. *J. Am. Chem. Soc.* **2019**, *141*, 14272–14279.

49. Wang, K.; Jia, Z.; Bai, Y.; Wang, X.; Hodgkiss, S. E.; Chen, L.; Chong, S. Y.; Wang, X.; Yang, H.; Xu, Y.; Feng, F.; Ward, J. W.; Cooper, A. I. Synthesis of Stable Thiazole-Linked Covalent Organic Frameworks via a Multicomponent Reaction. *J. Am. Chem. Soc.* **2020**, *142*, 11131–11138.

50. Wan, Y.; Wang, L.; Xu, H.; Wu, X.; Yang, J. A Simple Molecular Design Strategy for Two-Dimensional Covalent Organic Framework Capable of Visible-Light-Driven Water Splitting. *J. Am. Chem. Soc.* **2020**, *142*, 4508–4516.

51. Xu, J.; Yang, C.; Bi, S.; Wang, W.; He, Y.; Wu, D.; Liang, Q.; Wang, X.; Zhang, F. Vinylene-Linked Covalent Organic Frameworks (COFs) with Symmetry-Tuned Polarity and Photocatalytic Activity. *Angew. Chem. Int. Ed.* **2020**, *59*, 23845–23853.

52. Tu, T. N.; Nguyen, M. V.; Nguyen, H. L.; Yuliarto, B.; Cordova, K. E.; Demir, S. Designing Bipyridine-Functionalized Zirconium Metal–Organic Frameworks as a Platform for Clean Energy and Other Emerging Applications. *Coord. Chem. Rev.* **2018**, *364*, 33–50.

53. Leng, W.; Ge, R.; Dong, B.; Wang, C.; Gao, Y. Bimetallic Docked Covalent Organic Frameworks with High Catalytic Performance Towards Tandem Reactions. *RSC Adv.* **2016**, *6*, 37403–37406.

54. Gong, Y. N.; Zhong, W.; Li, Y.; Qiu, Y.; Zheng, L.; Jiang, J.; Jiang, H. L. Regulating Photocatalysis by Spin-State Manipulation of Cobalt in Covalent Organic Frameworks. *J. Am. Chem. Soc.* **2020**, *142*, 16723–16731.

55. Lu, C.; Zhang, P.; Jiang, S.; Wu, X.; Song, S.; Zhu, M.; Lou, Z.; Li, Z.; Liu, F.; Liu, Y.; Wang, Y.; Le, Z. Photocatalytic Reduction Elimination of UO_2^{2+} Pollutant Under Visible Light with Metal-Free Sulfur Doped g-C_3N_4 Photocatalyst. *Appl. Catal. B* **2017**, *200*, 378–385.

56. Vukovic, S.; Watson, L. A.; Kang, S. O.; Custelcean, R.; Hay, B. P. How Amidoxime Binds the Uranyl Cation. *Inorg. Chem.* **2012**, *51*, 3855–3859.

57. Wang, H.; Guo, H.; Zhang, N.; Chen, Z.; Hu, B.; Wang, X. Enhanced Photoreduction of U(VI) on C_3N_4 by Cr(VI) and Bisphenol A: ESR, XPS, and EXAFS Investigation. *Environ. Sci. Technol.* **2019**, *53*, 6454–6461.